CHINA FOUNDRY Research & Development
Vol. 19 No. 4 July 2022
www.springer.com/41230
https://doi.org/10.1007/s41230-022-1130-2

Simulation and experimental research on extra-squeeze forming method during gradient sand molding

Er-biao Jiang[1], *Zhong-de Shan[1,2], **Guang Cheng[1,3], Shao-zong Wang[1], Zhao-xian Gu[1], and Xin-lei Wang[1]

1. State Key Laboratory of Advanced Forming Technology and Equipment, China Academy of Machinery Science and Technology Group Co., Ltd., Beijing 100044, China

2. Nanjing University of Aeronautics and Astronautics, Nanjing 210016, China

3. Beijing Union University, Beijing 100101, China

Abstract: The flexible extrusion forming process (FEFP) is a sand mold patternless manufacturing technology that enables digital near-net shaping of complex sand molds. But, it is difficult to achieve the gradient sand molds with high surface strength and strong interior permeability by FEFP. To solve this problem, an extra-squeeze forming method based on FEFP for gradient sand mold was developed. To further reveal the extra-squeeze forming mechanism, based on the Johnson-Kendall-Roberts (JKR) theory and "gluing" notions, the single and double-sided squeeze models of gradient sand molds were established using the EDEM software. The squeezing processes of sand molds with different cavity depths of 60, 100, 140, 180, and 220 mm were systemically studied under single and double-sided squeeze conditions. The variation in the void fraction of sand mold as also investigated at a variety of extra-squeeze distances of 2, 3, 4, 5, and 6 mm, respectively. Simulation and test results show that a deeper cavity depth weakens the extrusion force transmission, which leads to a decrease in strength. The sand mold permeability and void fraction are identified to be positively correlated, while the tensile strength and void fraction appear to be negatively correlated. The void fraction of sand molds decreases with a longer extra-squeeze distance. A 6 mm extra-squeeze distance for the sand mold with 220 mm cavity depth results in a 26.8% increase in tensile strength with only a 5.7% reduction in the permeability. Hence, the extra-squeeze forming method can improve the quality of the sand mold by producing a gradient sand mold with high surface strength and strong interior permeability.

Keywords: patternless casting; gradient squeeze; sand mold performance; discrete element simulation; void fraction

CLC numbers: TG221 **Document code:** A **Article ID:** 1672-6421(2022)04-288-11

1 Introduction

Sand casting is one of the widely used casting methods in aerospace, national defense, military industry, automobiles, and shipbuilding fields. During the sand casting process, high-quality gradient sand molds with different strengths and permeability in different parts are essential for the formation of high-quality castings. The flexible extrusion forming process (FEFP) proposed by the China Academy of Machinery Science and Technology can produce high-quality sand molds with high efficiency and precision [1]. A schematic illustration of the FEFP technology is shown in Fig. 1. The process eliminates the preparation of a traditional casting mold made from wood or metal, and the mold repairing processes. Thus, it improves production flexibility and efficiency. The FEFP has significantly advantages in the production of high-end castings in small and medium batches with personalized customization [1-3]. A typical FEFP uses a single-sided squeeze method [1,4], then, due to the discontinuity in the force interaction between sand particles, the transmission of the extrusion force is easy to diverge [5,16]. For a deeper cavity, only a small extrusion force can be transmitted to the bottom of the cavity, as shown in Fig. 2(a), which can even create a void. In this case, the bottom and edges of the sand mold are prone to looseness, as shown in Fig. 2(b). Therefore, the FEFP with a single-sided squeeze method cannot

***Zhong-de Shan**

Male, born in 1970, Academician of Chinese Academy of Engineering, doctoral supervisor. His research interests mainly focus on digital mechanical equipment and advanced forming manufacturing technology. To date, he has published more than 80 papers and 4 books.

E-mail: shanzd@cam.com.cn

****Guang Cheng**

E-mail: chengguang@buu.edu.cn

Received: 2021-08-13; Accepted: 2022-04-29

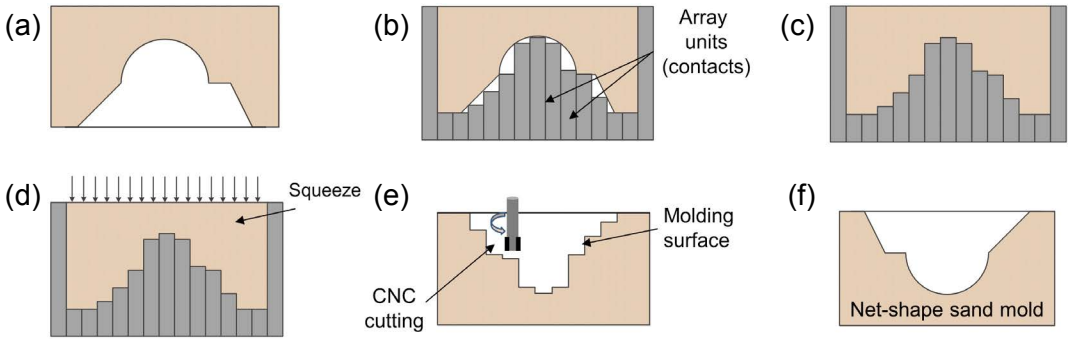

Fig. 1: Preparation for flexible extrusion forming process (FEFP) of sand mold [4]: (a) 3D CAD model; (b) near-shape adjustment of array unit; (c) sand filling; (d) squeeze, curing and demolding; (e) CNC cutting of near-shape sand mold; (f) net-shaped sand mold

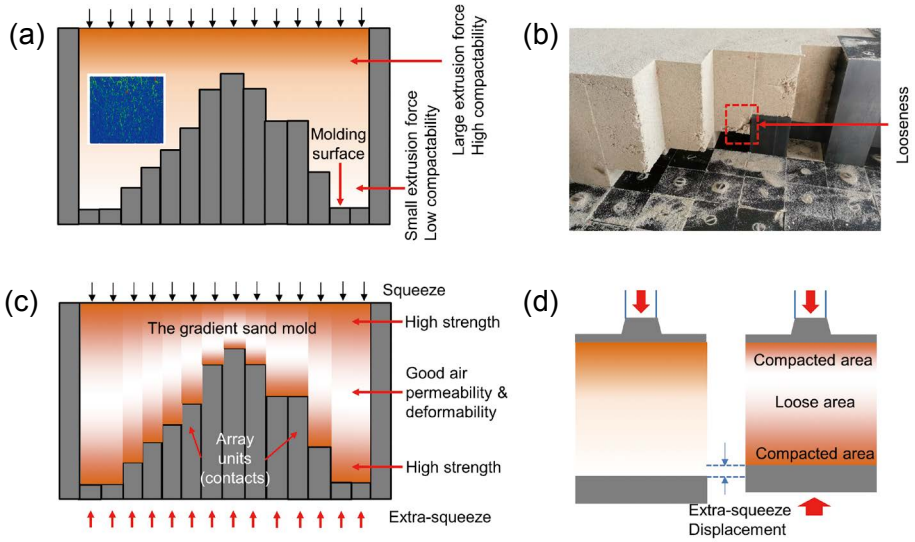

Fig. 2: Improvement for the near-shape process of sand mold: (a) single-side squeeze; (b) looseness at bottom and edges of the sand mold; (c) extra-squeeze method of the gradient sand mold (double-side); (d) extra-squeeze of a contact and gradient sand structure

prepare high-quality gradient sand molds with high surface strength and strong interior permeability.

Using extra-squeeze (double-sided squeeze) to control the compactness of the sand mold surface is a practical way of improving the quality of sand molds in the FEFP. Figures 2(c) and (d) show the extra-squeeze forming method for gradient sand mold. After the top of the sand mold is squeezed, the compactness of mold surface can be improved by rising contacts between array units with an extra-squeeze displacement. In the traditional compaction molding process with green sand, the method of sand filling with colored grids is often used to study the compaction effect, besides, the stress distribution can be explored by measuring the hardness, strength, density, and pressure [5, 15]. However, changes in the internal properties of the sand mold cannot be observed using these methods during the forming process. In recent years, with the improvement of the discrete element method (DEM) and computational tools, the use of DEM to simulate the sand mold forming process has attracted many attentions [6-9]. Chen et al. [10] studied the compaction characteristics of the clay sand and explored the corresponding DEM numerically by simulating the discontinuity of the sand compaction. He et al. [11, 12] proposed a GPU-based DEM for the large-scale discrete element simulation system, which significantly improved the computational efficiency of the model. Hovad et al. [13, 14] used the DEM to simulate the flow dynamics during a DISAMATIC green sand filling process with a good agreement with the experimental results. The above studies have mainly applied the DEM to conventional green sand molding, which reduced the number of tests and helped to observe the forming process. However, few works were found on the study of FEFP using the DEM in the resin sand forming process.

In this study, an extra-squeeze forming method for the gradient sand mold was proposed based on the FEFP. Based on the Johnson-Kendall-Roberts (JKR) theory and the notion of "gluing", a viscous sand particle action model was established to meet the properties of resin sand. To simulate the sand squeeze process with different cavity depths, a sand squeeze model with steps was designed. The DEM was applied to simulate the sand mold with varying cavity depths in the squeeze and extra-squeeze process. Finally, the accuracy of the model was verified experimentally.

2 Simulation methods and testing

2.1 Mechanical model of sand particles

2.1.1 Dynamic contact model

Since the contact between the sand particles is extremely complex in the forming process, a huge amount of calculation would be involved in simulation. For the convenience of calculation, the movement and collision between the particles were simplified as the interaction between softballs with a certain error range. The normal force between the particles was simplified as a spring and a damper, as illustrated in Fig. 3(a). The tangential force was simplified as a spring, a damper, and a slider, as illustrated in Fig. 3(b). According to the laws of kinematics, the following kinematic equations were established [16, 17]:

$$\begin{cases} M_i \dfrac{\mathrm{d}^2 S_{in}}{\mathrm{d}t^2} + \eta_n \dfrac{\mathrm{d}S_{in}}{\mathrm{d}t} + K_n S_{in} = \sum F_{in} \\ M_i \dfrac{\mathrm{d}^2 S_{i\tau}}{\mathrm{d}t^2} + \eta_\tau \dfrac{\mathrm{d}S_{i\tau}}{\mathrm{d}t} + K_\tau S_{i\tau} = \sum F_{i\tau} \\ I_i \dfrac{\mathrm{d}^2 \theta}{\mathrm{d}t^2} + \eta_n \dfrac{\mathrm{d}S_{in}}{\mathrm{d}t} + K_n S_{in} = \sum T \\ F_f = -\mu_c K_n S_{in} \end{cases} \tag{1}$$

where M_i is the mass of the sand particle i, I_i is the rotational inertia of the sand particle i. K_n and K_τ are the normal and tangential stiffness coefficients of the particle; η_n and η_τ are the damping coefficients of the particle in the normal and tangential direction, and θ is the angle of rotation of the particle during contact. Further, S_{in} and $S_{i\tau}$ are the displacement components in the normal and tangential directions of the particle i, respectively. F_{in} and $F_{i\tau}$ are the normal and tangential forces of the particle i, respectively, and T is the torque. μ_c is the friction coefficient of the particle, and F_f is the force of friction of the particle.

2.1.2 Mechanical model of sand particle bonding

During the curing process of resin sand by FEFP, sand particles were simplified as the spheres for modeling. The resin sand squeeze molding process was innovatively divided into the stages of squeezing and curing. The Hertz-Mindlin with the JKR cohesion model (hereinafter referred to as the JKR model [18]) was used to reflect the viscous characteristics of the resin and the particles. In the curing stage, the bonding bridge in the JKR model was simplified as a "glued" bond, as shown in Fig. 4(b). This bond can resist the tangential and normal movement. This bond breaks when the force between the particles is greater than the maximum tangential and normal allowable stress of the glued bond [19]. The mechanical model of the sand particle bonding is shown in Figs. 4(a) and (b).

Before curing, the force between the particles was determined using the JKR model. Once the curing time point was reached, the particles were connected by a "glued" bond. At this stage, the tangential force F_τ, normal force F_n and the torque were weakened, and the interaction between the particles was adjusted with the increasing time steps, thereby meeting the requirements mentioned in Eq. (2):

$$\begin{cases} \delta F_n = -v_n K_n A \delta_t \\ \delta F_\tau = -v_\tau K_\tau A \delta_t \\ \delta M_n = -\omega_n K_n J \delta_t \\ \delta M_\tau = -\omega_\tau K_\tau J \delta_t \end{cases} \tag{2}$$

where, R_b is the bonding radius, $A = \pi R_b^2$, $J = \frac{1}{2}\pi R_b^4$. δ_t is the time step, M_n and M_τ are the normal and tangential torque, ω_n and ω_τ are the normal and tangential angular velocity, and v_n and v_τ are the normal and tangential velocity, respectively. The adhesive bond breaks when the normal and tangential shear stresses (σ_{max} and τ_{max}) satisfy the following conditions:

$$\sigma_{max} < -\frac{F_n}{A} + \frac{2M_\tau}{J} R_b \tag{3}$$

$$\tau_{max} < -\frac{F_\tau}{A} + \frac{2M_n}{J} R_b \tag{4}$$

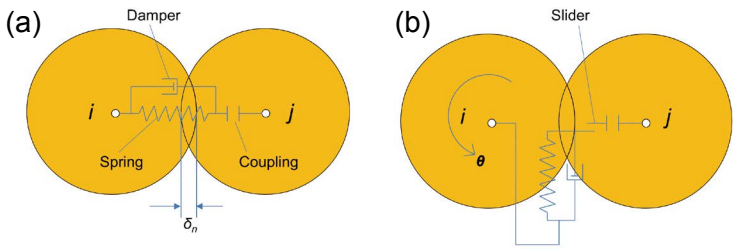

Fig. 3: Discrete element dynamics model: (a) normal force; (b) tangential force

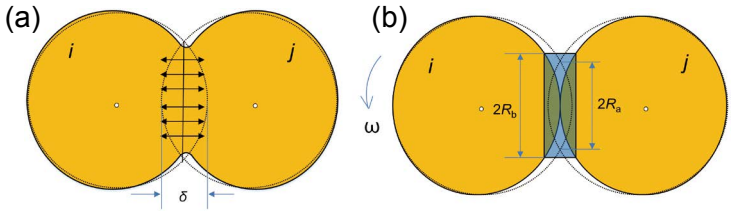

Fig. 4: Sand granular mechanical model: (a) JKR contact model; (b) bonding model

2.2 Simulation process

2.2.1 Setting of calculation parameters

In the DEM calculation, each particle corresponds to an element. Generally, the mesh number of the ordinary resin sand is 70–140, and the corresponding actual radius (r) is about 0.05–0.1 mm. Per kilogram sand contains about 130×10^6 sand grains [20]. Then, an amount of 35 kg is needed in the simulation. Based on the existing computing ability, it is difficult to calculate billions of particles. Therefore, within the allowable error range of the simulation results, the grains are usually coarsened in the particle model [21]. After parameter calibration [22] and experimental comparison, the radius of the simulated particle was set to be 50 times the real sand to facilitate the calculation. The "gluing" theory was used to simulate the curing of the sand molds. When the distance between the centers of the two particles is less than $0.1r$, the bond is formed with the bonded radius determined to be 4 mm. To avoid interference from the squeeze and extra-squeeze process, the curing simulation process started after 2.1 s. The main physical properties for a particle are listed in Table 1.

2.2.2 Establishment of simulated sand mold

To simulate the squeeze and extra-squeeze processes in the sand molds with different cavity depths, a sand box with steps was established using EDEM discrete element simulation software, as shown in Fig. 5(a). The cavity was 300 mm wide and 500 mm long with each step had a different depth. The cavity depth of the left half without extra-squeeze was in the range of 60–220 mm, while the right half was in the range of 62–226 mm (for extra-squeeze by 2, 3, 4, 5, and 6 mm). From the bottom to the top of the cavity, it was marked as Steps 1–5, as shown in Fig. 5(b). A virtual particle generation factory was established to fill the mold, as shown in Fig. 5(a). The filling time was 3.5 s and the particle generation rate was 10 kg·s^{-1}. The compressive force distribution of particles after generation is shown in Fig. 5(b).

2.3 Test materials and equipment

In this experiment, 70–140 mesh silica sand was used as molding sand. The particles have a shape similar to a sphere, as shown in Fig. 6(a). The particles show a normal size distribution, as shown in Fig. 6(b), with the peak particle size

Table 1: Main properties of the molding sand

Main properties	Value	Main properties	Value
Mean radius (r)	4.98 mm	Rolling friction coefficient	0.15
The standard deviation of particle distribution	0.02	Quality of simulated sand	35.0659 kg
Particle density (ρ)	2,600 kg·m^{-3}	Initial speed	2 m·s^{-1}
Poisson's ratio of granular materials	0.2	Time-step in the simulation	3.00e-06 s
Shear modulus of granular material	4.2e+10 Pa	Acceleration of gravity	9.8 m·s^{-2}
Coefficient of restitution	0.5	Mesh size	3r
Coefficient of static friction	0.7	Maximum number of placement attempts	20
Surface energy	0.043 J·m^{-2}	Sand box material density	7,800 kg·m^{-3}

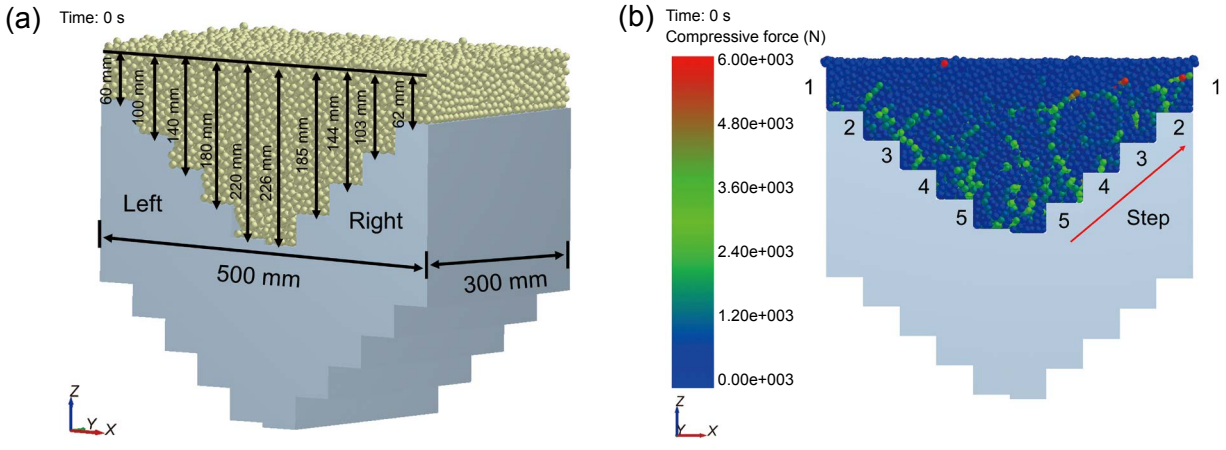

Fig. 5: Size of sand box (a), and compressive force distribution after generation of sand grains (b)

observed to be 199.2 μm. Phenolic resin NP-101HB was used as the binder with the curing agent of NP-102HB. Their contents were both 1wt.% of the molding sand. The catalyst NP-103E (0.6wt.% of the binder) was added to the binder. The S20 bowl-type sand mixer was utilized to mix above materials for 25 s.

A digital flexible squeeze molding machine CAMTC-DCMFP-2000, developed by the China Academy of Machinery Science and Technology, was used to squeeze the test materials into the near-shape sand molds. The maximum manufacturing size of the molding machine is 2,000 mm×1,500 mm×300 mm, whereas the cross-sectional size of the array contacts [Fig. 1(b)] is 50 mm×50 mm. There are a total of 1,200 array contacts. Further, a digital precision patternless cast forming machine (CAMTC-SMM1500S), also developed by the China Academy of Machinery Science and Technology, was used to mill the near-shape sand molds to obtain the specimens.

2.4 Forming process, sample processing, and testing

(1) First, a 3D CAD model was recognized by the computer. The near-shape data of the sand mold was calculated by the near-shape algorithm, and then imported into the digital flexible squeeze molding machine.

(2) The array contacts of the digital flexible extrusion forming machine were adjusted to form a flexible sand box with steps defined by the data file, as shown in Fig. 7(a).

(3) After sand filling, compaction, and curing, the near-shape sand mold blocks with steps were released, as shown in Figs. 7(b) and (c).

(4) The specimen data file was imported into the computer, and the CAMTC-SMM1500S sand mold digital precision patternless cast forming machine was used to process the near-shape sand mold blocks. Subsequently, the tensile "8" samples, as well as the Φ50 mm×50 mm air permeability specimens, were cut out.

(5) The SQS-II intelligent sand strength tester and STD electric air permeability tester were used to explore the tensile strength and air permeability of each step of the sand mold, respectively.

3 Results and discussion

3.1 Effect of squeeze process on stepped mold

After the particles were generated, the virtual particle generation factory was removed, and a simulated squeeze plate with a dimension of 500 mm×300 mm was set up, as shown in Fig. 8(a). The squeeze plate vertically moves downwards at an initial speed (v) of 12 mm·s^{-1}. The squeeze process at the squeeze time of 0, 0.5, 0.75, and 1 s is illustrated in Fig. 8. At 0.5 s [Fig. 8(b)], the squeeze plate moves downwards. As the particles are relatively loose at this stage, the particles are easy to be displaced and re-arranged. As a result, the compressive stress among the particles is not obvious. At 0.75 s [Fig. 8(c)], as the squeeze plate continues to move downwards, the particles at the top of the simulated sand mold are dislocated and re-arranged with distinctive pressure applied on the particles. The compressive stress is more focused on the top parts. By increasing the squeeze time to 1 s [Fig. 8(d)], the squeeze process is completed. The overall simulation shows a high pressure on the top and low pressure at the bottom.

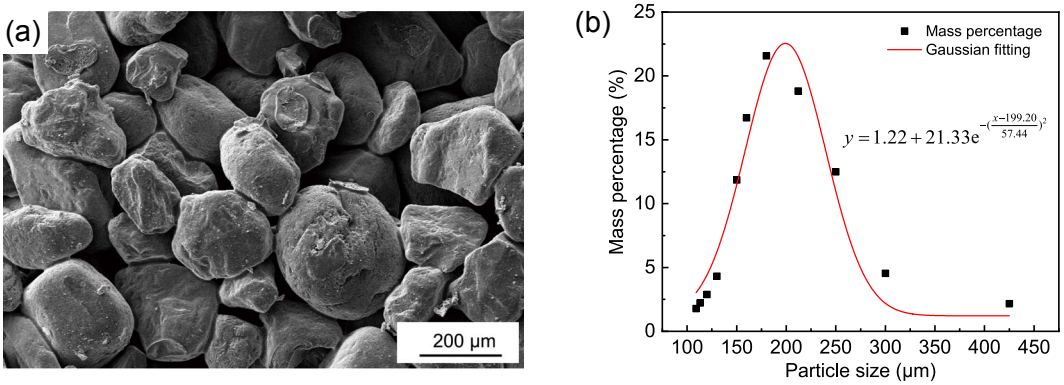

Fig. 6: Micro-morphology (a) and size distribution (b) of the silica sand

Fig. 7: Preparation of near-shape blocks: (a) shape adjustment; (b) compaction; (c) near-shape sand mold

To analyze the changes in the normal force in the squeeze process, the overall normal force of the simulated sand mold was monitored. Figure 9 shows the change in the chain of normal force before and after the squeeze. The bottom pressure of the mold is relatively high before the squeeze process, although the absolute normal force is small and less than 2 N. However, after squeezing for 1 s, as shown in Fig. 9(b), the normal force at the top edge of the 1st step of sand mold becomes dominant due to the shallow cavity. From the 3rd step (about 150 mm) of the simulated sand mold, the force chain is almost disappeared.

Figure 10 shows the nephogram of the compressive force of the sand mold during the squeeze process and the change of void fractions in different steps with time. It can be seen from Fig. 10(a) that the compressive force gradually increases from Step 5 to Step 1. However, in Fig. 10(b), it can be found that the void fraction gradually decreases with time during the squeezing. The void fraction of the Step 1 is rapidly decreased by 9.6% from 41.8% at the beginning to 36.9% at about 1 s with the fastest reduction rate, resulting in the smallest void fraction. Step 1, which is close to the squeeze plate, has the smallest cavity depth. During the squeeze process, the force on the Step 1 is the largest, so the physical deformation is more obvious compared with other steps, leading to a rapid decrease in the void fraction in the sand mold.

3.2 Effect of extra-squeeze on stepped mold

As shown in Fig. 9(b), after 1 s squeezing, the bottom pressure of the simulated sand mold is still relatively small. This is due to the weak extrusion force transfer between the steps, which is dissipated between the sand particles. Hence, the bottom of the sand mold is loose and prone to the formation of voids. To

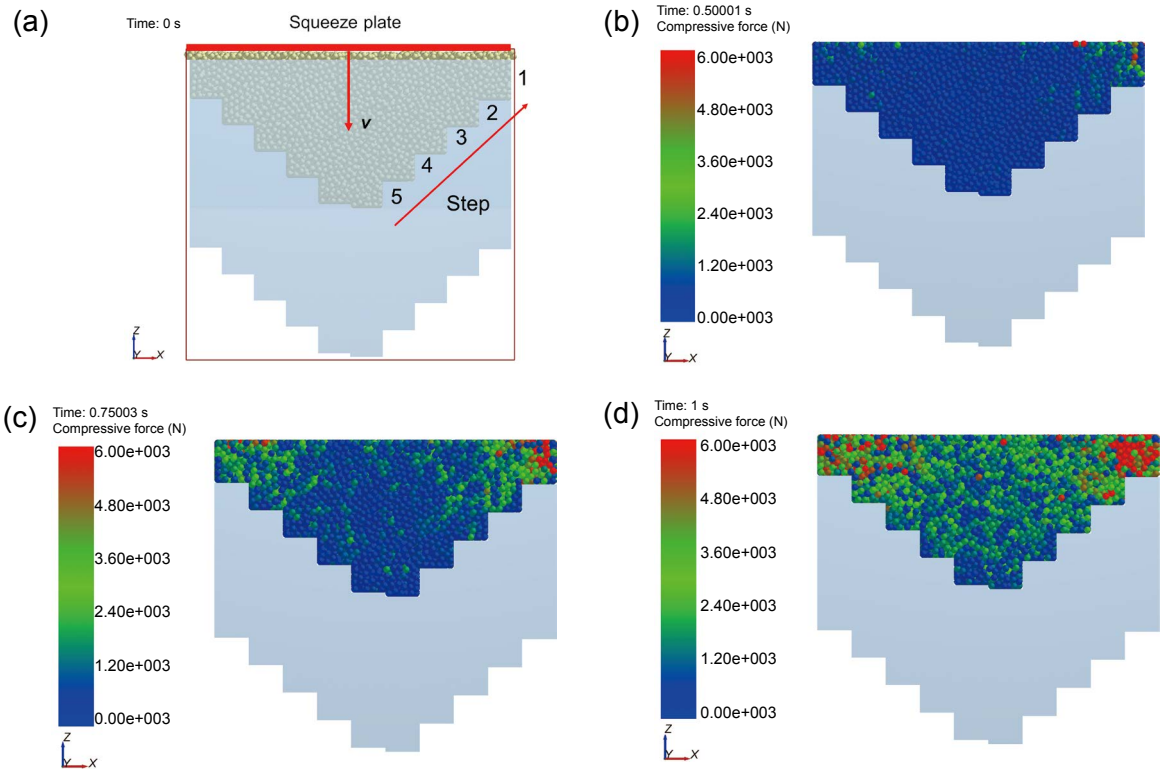

Fig. 8: Squeeze process: (a) *t*=0 s; (b) *t*=0.5 s; (c) *t*=0.75 s; (d) *t*=1 s

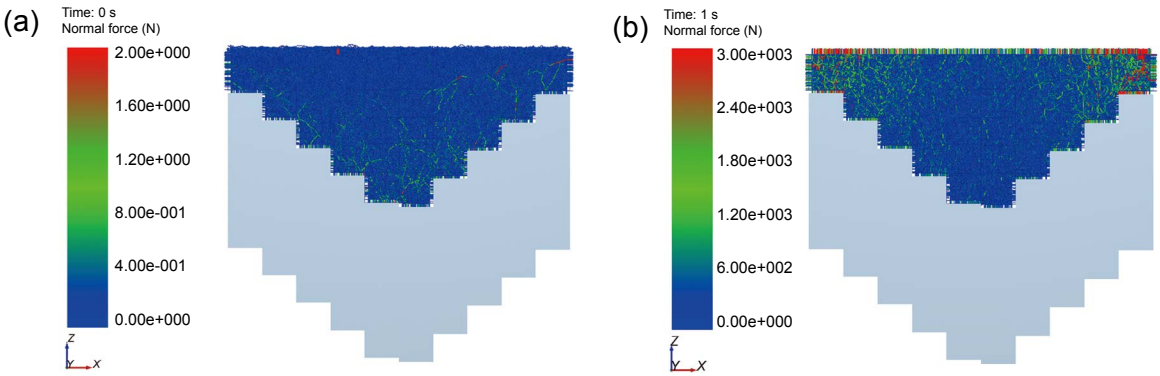

Fig. 9: Chain of normal force: (a) chain of normal force before squeezing at 0 s; (b) chain of normal force after squeezing at 1 s

overcome this problem, the simulation continues to carry out the pressure compensation with extra-squeeze on the lower right side of the simulated sand mold. As shown in Figs. 11, the steps on the right side were sequentially compensated (extra-squeeze) by 6, 5, 4, 3, and 2 mm from the bottom to the top starting from 1 s, and the extra-squeezing time is 1 s. The change in the normal force before and after extra-squeeze is depicted in Fig. 11. Before the pressure compensation, the normal force distributions on the left and right sides are identical, as shown in Fig. 11(a). The normal force on the right side steps increases after the extra-squeeze, as shown in Fig. 11(b). To study the effects of extra-squeeze on the mold, the change of void fraction of the sand mold with and without pressure compensation is shown in Figs. 10 and 12. The dimensions of the samples for Steps 1–5 are 300 mm× 50 mm× 50 mm, respectively.

The void fraction from the 1st to the 5th step on the left side of the simulated sand mold (without pressure compensation) is generally stable from 1–1.6 s, as shown in Fig. 10(b). After pressure is applied to the right half of the simulated sand mold, the overall void fraction increases firstly followed by a sharp decline, which finally becomes stable when the pressure compensation is finished, as shown in Fig. 12(b). To explain this process precisely, the total force from monitoring Area 4 on

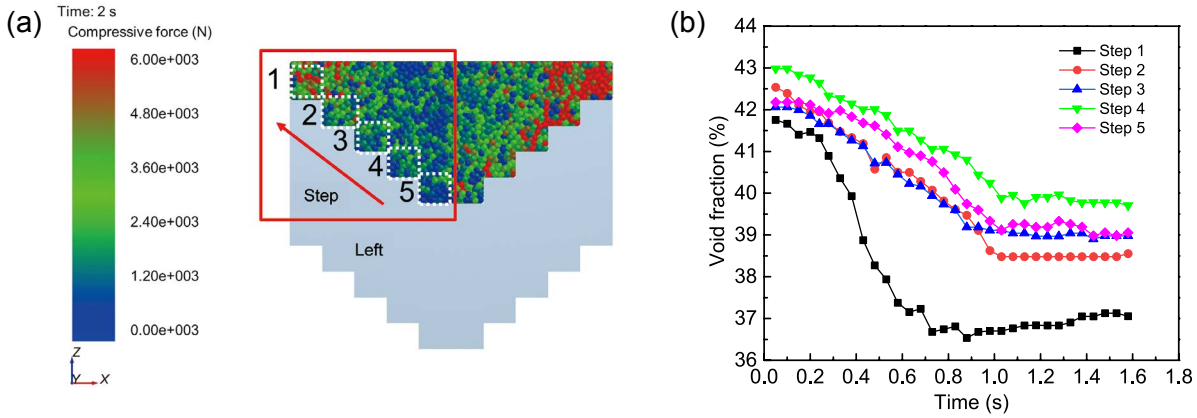

Fig. 10: Nephogram of compressive force of the sand mold (a), and variation in the void fraction of the left half over time during the squeeze process (b)

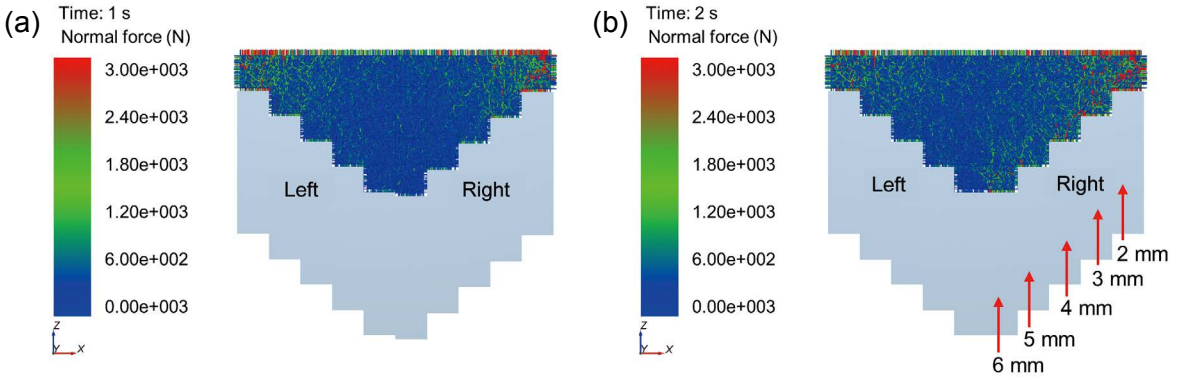

Fig. 11: Normal force variation of the right half mold without (a) and with extra-squeeze process (b)

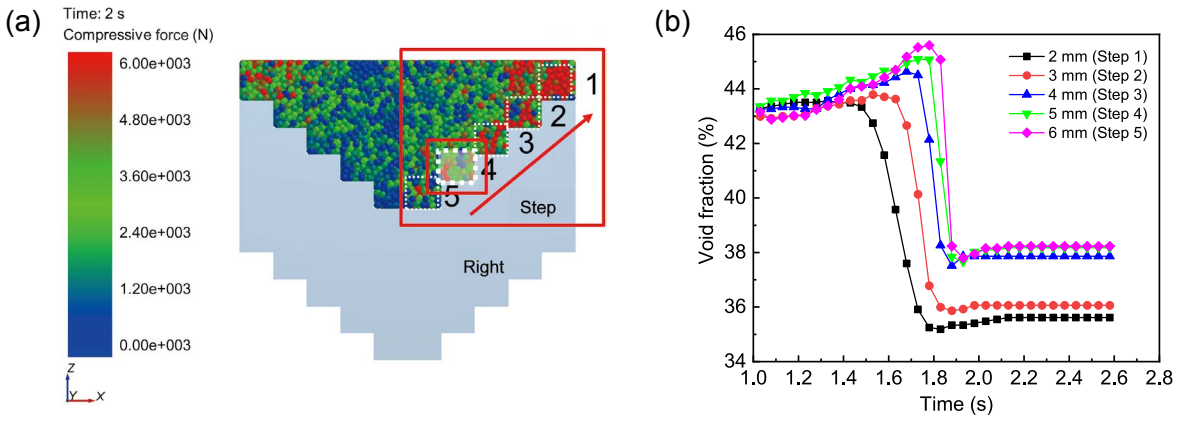

Fig. 12: Nephogram of compressive force of the sand mold (a) and void fraction of the right half mold vs. time with extra-squeeze process (b)

right half [Fig. 13(a)] was measured and shown in Figs. 13(b) and (c). The total force increases during both the squeeze and extra-squeeze processes. However, during the extra-squeeze process, the total force in Area 4 presents a linear increase from 1 s to 1.8 s. During this process, the "incompact" particles at the bottom of Area 4 continue to rise and the "compact" particles at the top of Area 4 were pushed out, causing a slowly increase in void fraction. Then, there is a rapid increase in the total force from 1.8 s to 1.9 s as the extra-squeeze continues [Fig. 13(c)]. During the period of 1.8–1.9 s , these "incompact" particles are more strongly constrained by the particles at the top of Area 4 than they are during the 1 s to 1.8 s period, so the particles are rearranged, resulting in a sharp drop in void fraction (in Step 4), as shown in Fig. 12(b).

The change of void fraction with the five steps is shown in Fig. 12(b). After 2 mm extra-squeeze of the 1st step on the right, with the smallest distance from the pressure plate, the pressure increases significantly. Thus, the observed variation is large during the pressure compensation process. As the particles arrangement is still relatively loose, the void fraction varies greatly with the extra-squeeze. However, due to the deeper cavity, the final void fraction of the 3rd, 4th and 5th steps is still larger than that of the 1st step [Fig. 12(b)]. At the same time, it is noted that the voids of the 3rd, 4th and 5th steps are similar after extra-squeeze, indicating that the extra-squeeze distances might be insufficient.

3.3 Same cavity depth squeeze and extra-squeeze process and analysis

To obtain the squeeze and extra-squeeze behaviors for the same cavity depth, the middle area of the simulated sand mold was also monitored. In addition, the void fraction of the middle zone (left) [Fig. 14(a)] was calculated. As shown in Fig. 14(b), with a 220 mm cavity depth, the void fraction of all steps decreases gradually with an increase in squeezing time. The first step exhibits the greatest change due to the small cavity depth and being close to the squeeze plate. Especially as the squeeze time increases from 0.9 s to 1.0 s, the void fraction rapidly decreases from 41.6% to 38.1%.

The void fraction of the middle zone (right) [Fig. 15(a)] was also calculated. After the 5th step of the sand mold is extra-squeezed for 6 mm, the void fraction of the 5th step first increases from 43.2% to 45.6%, followed by a sharp decrease to 38.2%, as shown in Fig. 15(b), while the void fraction of the other steps shows a relatively slow decreasing trend. Figure 16 shows the change of void fraction at different steps in the middle area (cavity depth of 220 mm) with and without extra-squeezing. It can be seen that the void fraction of Steps 1–5 shows an overall gradient distribution with small on both sides (Step 1, Step 5) and large in the middle (Steps 2–4) after extra-squeeze. The void fraction of the first step is smaller than that of the fifth step. Nevertheless, it nearly meets the ideal gradient requirement, which requires the void fraction in the fifth step

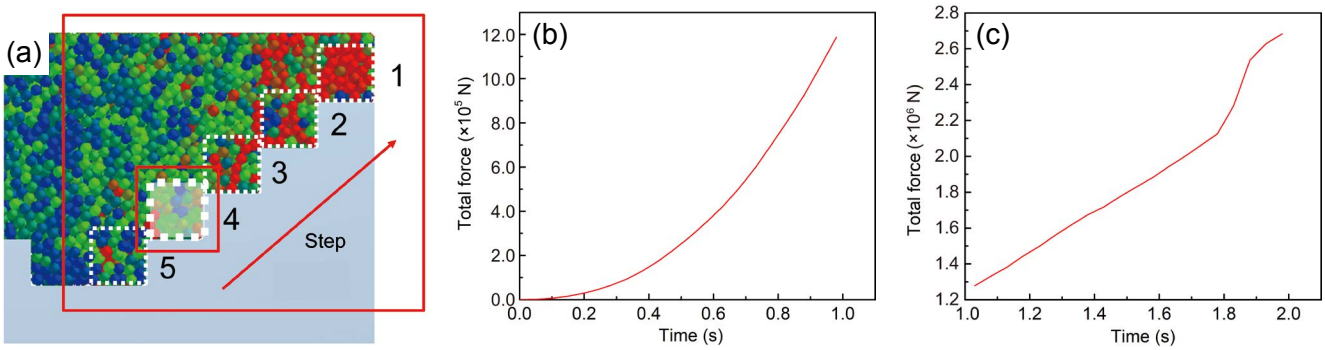

Fig. 13: Variation in the total force betwen the squeeze (b) and extra-squeeze (c) processes of the right monitoring Area 4 (a)

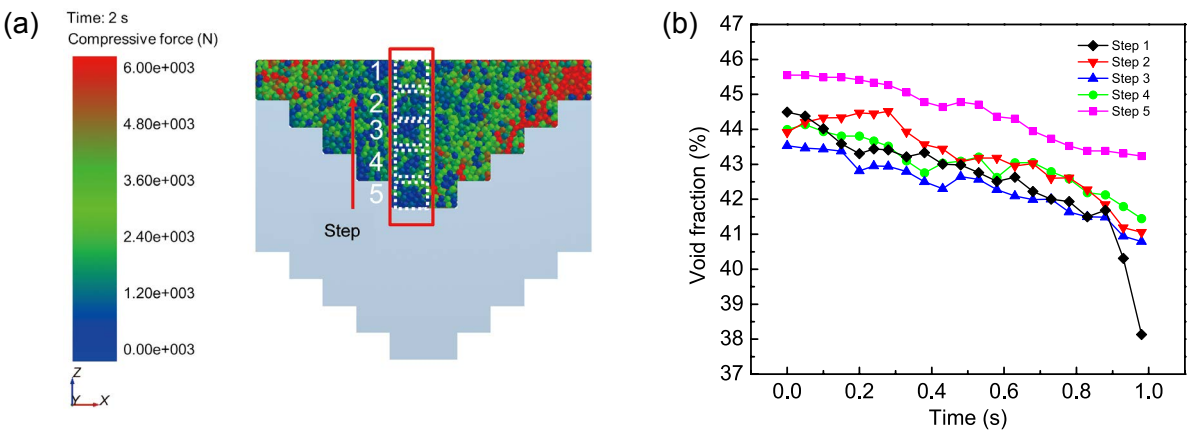

Fig. 14: Compression force of middle zone (left) (a) and trend of the void fraction in the middle zone (left) during the squeeze process (b)

to be smaller than that of the first step and the strength of the parting surface (Step 5) should be greater than the surface strength of the sand mold. The reason for that maybe the deformation of the first step is larger, and the compactness of the first step is higher than that of Step 5 after being squeezed. The other reason is that the squeeze force transmission effect gradually decreases from Steps 1 to 5.

3.4 Experimental results

The tensile strength sampling position is shown in Fig. 17(a) with 6 steps, while the permeability sampling position is shown in Fig. 17(b) with 4 steps. Tensile strength and air permeability of the specimens of each step of the sand mold were analyzed. As shown in Fig. 18, when the pressure is not compensated at the cavity depth of 220 mm, the tensile strength decreases with the increase of the step, which is consistent with the squeeze force transmission behavior in the simulation. After applying the extra pressure, the void fraction is reduced, but the tensile strength is improved. Combined with Fig. 16, it can be found the smaller the void fraction, the higher the strength. The tensile strength of the 6th step is increased by 26.8% from 1.42 MPa without extra squeeze to 1.80 MPa with extra squeeze. This increase is significant, although its value is still slightly lower than that of the first step (1.86 MPa). While, due to the limited squeeze force transmission distance, change in the void fraction of Steps 3 and 4 is small, and the tensile strength is correspondingly low. Therefore, the tensile strength of Steps 1–6 exhibits a high-low-high gradient distribution, as shown in Fig. 18(a). This result preliminarily meets the proposed requirements of "gradient", i.e., a medium-low-high gradient distribution of tensile strength.

The strength of the sand mold edge after extra-squeezing is generally higher than the uncompensated one. The 1st step offers the largest strength, the 5th step offers the smallest strength, as shown in Fig. 18(b). This is also opposite to the changing trend of the void fraction. As shown in Fig. 18(a), the overall tensile strength of each step for the 220 mm cavity depth increases after extra squeeze, which is consistent with the trend of the normal force for different cavity depths. As shown in Fig. 11(b), the normal force at the edge is larger than that of the middle at the same depth. Thus, the edge is relatively more compact, resulting in a high tensile strength. The 1st step with the smallest cavity depth presents the most transmission of the squeeze force in association with the largest tensile strength before and after the pressure

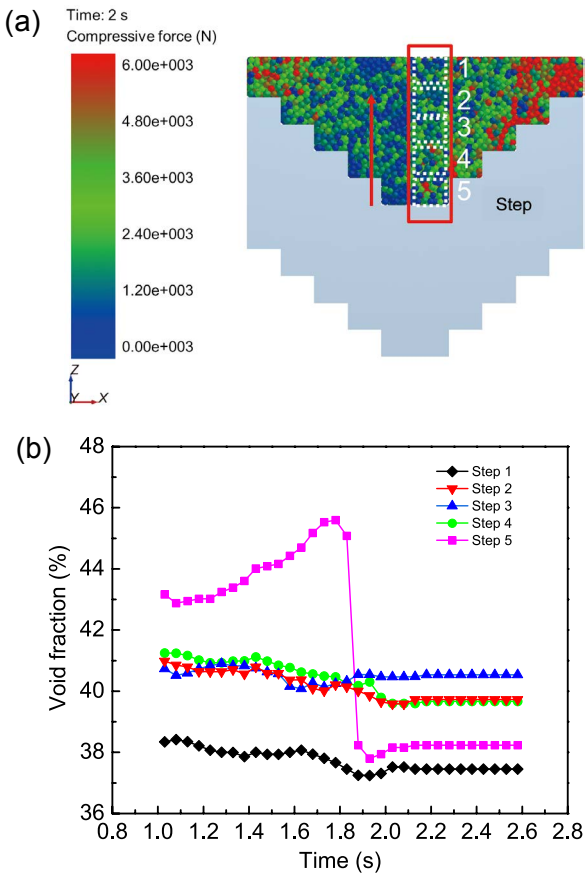

Fig. 15: Compression force of middle zone (right) (a) and trend of the void fraction during the extra-squeeze process (b)

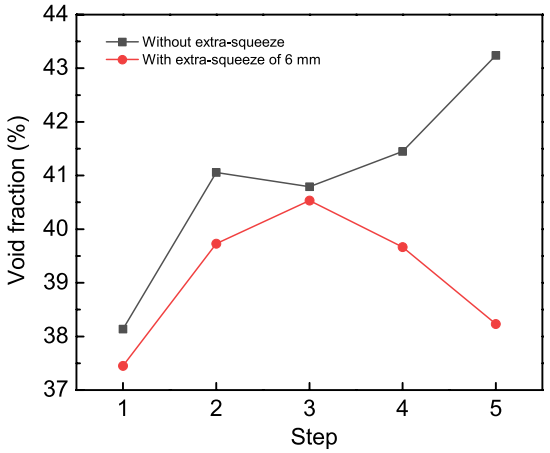

Fig. 16: Change of void fraction at different steps in the middle area with and without extra-squeeze

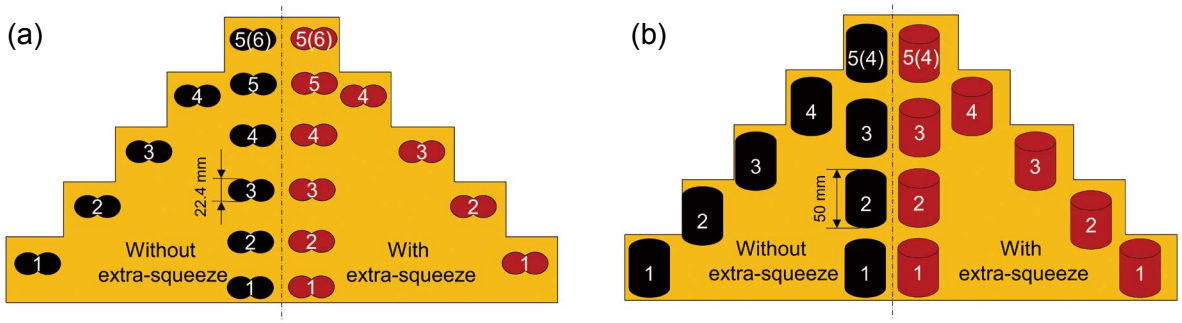

Fig. 17: Tensile strength sampling position (a) and permeability sampling position (b)

compensation. Meanwhile, the strength gradually decreases with the increase of the number of steps. However, due to the different extra-squeeze distances at the different depths of the cavity, the optimal pressure compensation distance for each step cannot be determined. Further pressure compensation tests will be conducted for the same cavity depth.

The air permeability test was carried out on each step of the sand mold. It is observed that the overall air permeability of the sand mold is higher before the extra pressure is applied. When the pressure is not compensated, the air permeability increases with the increase of the cavity depth. This is opposite to the trend of tensile strength. However, it is consistent with the changing trend of the void fraction. As the depth of the cavity increases, the squeeze force transmission becomes less effective, which leads to a large void fraction with enhanced air permeability. The air permeability of Steps 1–4 is increased from 162 to 175 without pressure compensation, increased by 8%, as shown in Fig. 19(a). Meanwhile, the tensile strength is decreased by 13%, from 1.64 to 1.42 MPa [Fig. 18(a)]. Taking into account the negative correlation between the strength and air permeability of the sand mold, an appropriate increase in the strength of the sand mold with a small decrease in air permeability can improve the overall performance of the sand mold.

For a cavity depth of 220 mm, after extra-squeeze by 6 mm, the air permeability of the sand mold is decreased slightly in comparison with the mold without pressure compensation, as shown in Fig. 19(a). For instance, the air permeability of the 4th step is reduced from 175 to 165 (5.7%), much less than the 26.8% increase in strength. Hence, it is possible to achieve high strength without sacrificing permeability.

At the edge of the sand mold, the air permeability after extra-squeeze is generally also lower than that without extra-squeeze. The air permeability of Steps 1–5 is increased gradually, as shown in Fig. 19(b), which is consistent with the change of the void fraction. However, it is opposite to the trend of the tensile strength at the edge after extra-squeeze. Compared with Fig. 19(a), the air permeability at the edge of the sand mold is generally smaller than that in the middle. As the normal force at the edge is greater than that in the middle of the same cavity depth, the edges are more compact, resulting in a reduced air permeability, which is opposite to the changing trend of tensile strength.

The analysis of the tensile strength and air permeability reveals that after applying the extra pressure, the strength of each step of the sand mold is enhanced, and the air permeability is reduced. Significant changes in the tensile strength are observed after the pressure compensation at the edge of the sand mold. However, only a small change is observed for the air permeability. For the gradient sand molds, the increase in strength of the parting surface ensures that the mold is not damaged or deformed during the modeling and handling processes. In addition, it also ensures a small reduction in air permeability.

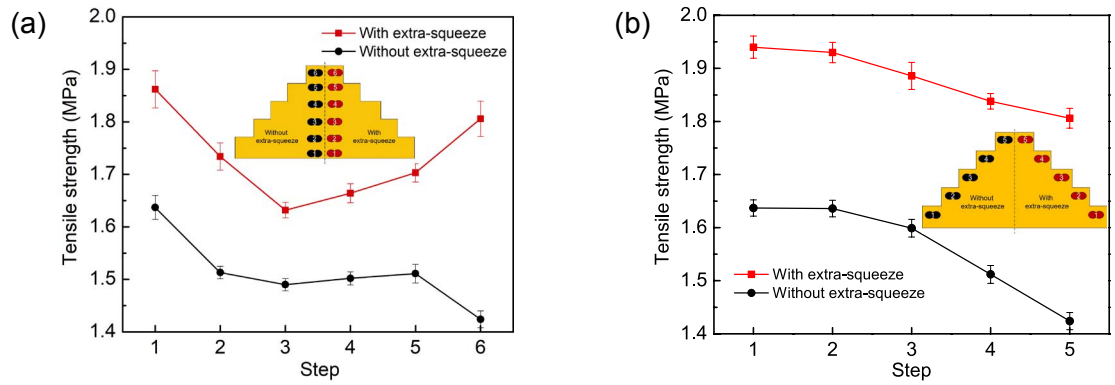

Fig. 18: Tensile strength of each step at 220 mm cavity depth (a), and tensile strength at different cavity depths with and without extra-squeeze (b)

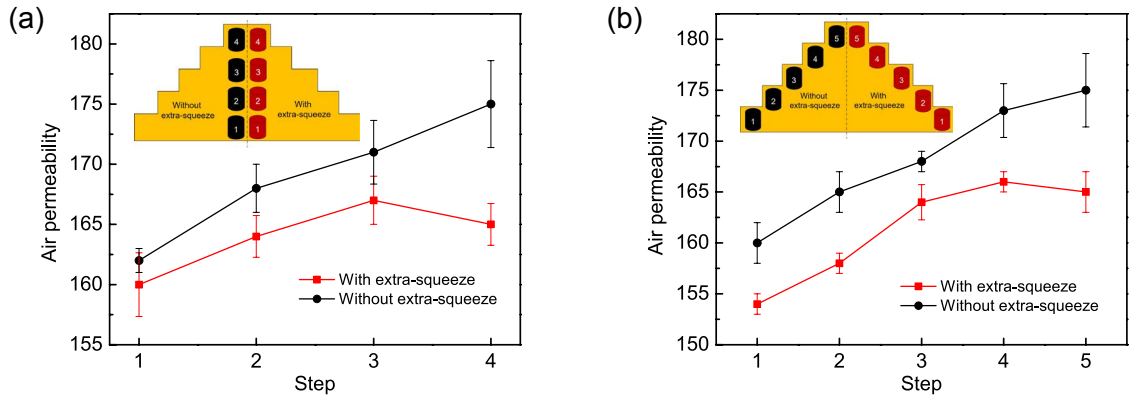

Fig. 19: Permeability of each step at a cavity depth of 220 mm (a), and permeability of different cavity depths with and without extra-squeeze process (b)

4 Conclusions

Based on the JKR and "gluing" theories, the contact dynamics and bonding mechanics models of the sand particles were established. The gradient sand molding process is innovatively divided into two stages: squeeze and pressure compensation. DEM is utilized to simulate the squeeze and extra-squeeze forming processes for the FEFP of the gradient sand mold. The results are verified experimentally. The conclusions can be drawn as follows:

(1) Owing to the limited squeeze force transmission, the bottom of the deep cavity sand mold is less compact or hardly squeezed. In case the cavity depth exceeds 150 mm, the bottom of the sand mold is prone to looseness. Adopting the extra-squeeze forming method can effectively avoid the defects at the bottom and prepare the gradient sand mold with high surface strength while remaining good internal air permeability.

(2) Combining with the discrete element simulation results, the sand mold performance is successfully explored for the cavity depths of 60, 100, 140, 180, and 220 mm with extra-squeeze by 2, 3, 4, 5, and 6 mm, respectively. It is observed that the performance of the sand mold is consistent with the simulation results. The sand molds with different cavity depths need to be compensated correspondingly to achieve the desired property. More specifically, with the increase of cavity depth, more extra-squeezed distance is needed. A 6 mm extra-squeeze on the sand mold with the 220 mm cavity depth increases the tensile strength by 26.8% with a limited reduction of the air permeability by 5.7%. The use of extra-squeeze increases the strength of the sand mold while maintaining good air permeability.

(3) The tensile strength performance of the sand mold is negatively correlated with the change of the void fraction. However, the change of the void fraction is positively correlated with permeability. A longer extra-squeeze distance decreases the void fraction and air permeability but increases the strength. The changing trend of the void fraction can provide useful guidelines for the FEFP of the gradient sand molds.

Acknowledgements

This work was financially supported by the National Innovation Center Fund of Lightweight Material Forming Technology and Equipment (No. 111902Q-D), the State Key Laboratory Fund of Advanced Forming Technology and Equipment (No. SKL2020008), and the National Key Research and Development Program (No. 2020YFF0217703).

References

[1] Shan Z D. Patternless casting. Beijing: China Machine Press, 2017: 13–17. (In Chinese)
[2] Shan Z D, Yang H Q, Liu F. et al. Performance of digital patternless freeze-casting sand mould. China Foundry, 2020, 17(4): 308–313.
[3] Liu L M, Shan Z D, Lan D, et al. Research of cutting properties of mold sand based on the precision forming technology without pattern. Foundry, 2016, 65(12): 1167–1171. (In Chinese)
[4] Shan Z D, Zhang S, Gu Z X. Optimization algorithm research of near-net forming sand mold with digital flexible extrusion technology. Journal of Mechanical Engineering, 2016, 52(13): 149–155.
[5] Xie B. A study on the green sand stress field in squeeze mounding and air impact moulding. Doctoral Dissertation. Beijing: Tsinghua University, 1993: 42–47.
[6] Tsuji Y, Kawaguchi T, Tanaka T. Discrete particle simulation of two-dimensional fluidized bed. Powder Technology, 1993, 77(1): 79–87.
[7] Parteli E J, Schmidt J, Blümel C, et al. Attractive particle interaction forces and packing density of fine glass powders. Scientific Reports, 2014, 4: 6227.
[8] Cheng K, Wang Y, Yang Q, et al. Determination of microscopic parameters of quartz sand through tri-axial test using the discrete element method. Computers and Geotechnics, 2017, 92: 22–40.
[9] Maeda Y, Ito Y, Yoshida S, et al. Effects of green sand particle distribution on squeeze compacting behavior analyzed by discrete element method. International Journal of Metalcasting, 2019, 13(3): 546–552.
[10] Chen X P, Nomura H, Maeda Y. Analysis of green sand composition process applying Cooper-Eaton model. Journal of the Korea Foundry Society, 2004, 24(3): 35–41.
[11] He Y, Evans T J, Yu A B, et al. A GPU-based DEM for modelling large scale powder compaction with wide size distributions. Powder Technology, 2018, 333: 219–228.
[12] He Y, Hassanpour A, Behjani M A, et al. A novel stiffness scaling methodology for discrete element modelling of cohesive fine powders. Applied Mathematical Modelling, 2021, 90: 817–844.
[13] Hovad E, Spangenberg J, Larsen P, et al. Simulating the DISAMATIC process using the discrete element method – A dynamical study of granular flow. Powder Technology, 2016, 303: 228–240.
[14] Hovad E. Numerical simulation of flow and compression of green sand. Doctoral Dissertation. Lyngby: Technical University of Denmark, 2017: 8–18.
[15] Li R D, Mi G F. Casting technology. Beijing: China Machine Press, 2013: 17–20. (In Chinese)
[16] Sun Q C. Wang G Q. Introduction to particle mechanics (hardcover). Beijing: Science Press, 2009: 15–43. (In Chinese)
[17] Guo Z. 3D printing forming methodology of multi-material sand mold. Doctoral Dissertation. Beijing: Tsinghua University, 2019: 52–55.
[18] Johnson K L, Kendall K, Roberts A D. Surface energy and the contact of elastic solids. Procrsoclonda, 1971, 324(1558): 301–313.
[19] Potyondy D O, Cundall P A. A bonded-particle model for rock. International Journal of Rock Mechanics and Mining Sciences, 2004, 41(8): 1329–1364.
[20] Maeda Y, Maruoka Y, Makino H, et al. Squeeze molding simulation using the distinct element method considering green sand properties. Journal of Materials Processing Technology, 2003, 135(2–3): 172–178.
[21] Feng Y T, Han K, Owen Y, et al. On upscaling of discrete element models: Similarity principles. Engineering Computations: International Journal for Computer-Aided Engineering, 2009, 26(6): 599–609.
[22] Feng Y T, Owen D R J. Discrete element modelling of large scale particle systems – I: Exact scaling laws. Computational Particle Mechanics, 2014, 1(2): 159–168.